

1 **Bottom-Up Synthesis of Carbon Nanoparticles with Higher**

2 **Doxorubicin Efficacy**

3 Samer Bayda^{a,b}, Mohamad Hadla^{a,c}, Stefano Palazzolo^{a,b}, Vinit Kumar^a, Isabella Caligiuri^a,
4 Emmanuele Ambrosi^{d,e}, Enrico Pontoglio^{d,e,f}, Marco Agostini^{g,h}, Tiziano Tuccinardiⁱ, Alvise
5 Benedetti^{d,e}, Pietro Riello^{d,e}, Vincenzo Canzonieri^a, Giuseppe Corona^a, Giuseppe Toffoli^a and
6 Flavio Rizzolio^{a*}

7 a. Department of Translational Research, National Cancer Institute - CRO-IRCCS,
8 Aviano, Italy

9 b. Doctoral School in Nanotechnology, University of Trieste, Italy

10 c. Doctoral School in Pharmacological Sciences, University of Padova, Italy

11 d. Department of Molecular Sciences and Nanosystems and Electron Microscopy Center
12 “Giovanni Stevanato”, University Ca’ Foscari of Venezia, Italy

13 e. European Center of Living Technology, Venezia-Mestre, Italy

14 f. Doctoral School in Chemistry, University of Trieste, Italy

15 g. Department of Surgical, Oncological and Gastroenterological Sciences, Section of
16 Surgery, University of Padova, Italy

17 h. Pediatric Research Institute-Città della Speranza, Padova, Italy

18 i. Department of Pharmacy, University of Pisa, Italy

19 *** Corresponding Authors:**

20 Flavio Rizzolio, PhD. Tel. +39-0434 659384; Fax. +39-0434 659799. E-mail: frizzolio@cro.it;
21 Clinical Pharmacology, Department of Molecular Biology and Translational Research, National
22 Cancer Institute and Center for Molecular Biomedicine, CRO Aviano (PN), Via Franco Gallini, 2,
23 Aviano 33081 - PN - Italy.

24 **Keywords:** Carbon Nanoparticles, Cancer, Drug delivery, Nanotechnology, Doxorubicin.

25 **Abstract**

26 Nanomedicine requires intelligent and non-toxic nanomaterials for real clinical applications.
27 Carbon materials possess interesting properties but with some limitations due to toxic effects.
28 Interest in carbon nanoparticles (CNPs) is increasing because they are considered green
29 materials with tunable optical properties, overcoming the problem of toxicity associated with
30 quantum dots or nanocrystals, and can be utilized as smart drug delivery systems. Using
31 black tea as a raw material, we synthesized CNPs with a narrow size distribution, tunable
32 optical properties covering visible to deep red absorption, non-toxicity and easy synthesis for
33 large-scale production. We utilized these CNPs to label subcellular structures such as
34 exosomes. More importantly, these new CNPs can escape lysosomal sequestration and
35 rapidly distribute themselves in the cytoplasm to release doxorubicin (doxo) with better
36 efficacy than the free drug. The release of doxo from CNPs was optimal at low pH, similar to
37 the tumour microenvironment. These CNPs were non-toxic in mice and reduced the tumour
38 burden when loaded with doxo due to an improved pharmacokinetics profile. In summary, we
39 created a new [delivery](#) system that is potentially useful for improving cancer treatments and
40 opening a new window for tagging microvesicles utilized in liquid biopsies.

41 **Introduction**

42 Nanoparticle technology is an attractive field at the forefront of research and plays important
43 roles in medicine, agriculture and electronics. Nanoparticles have wide applications in
44 medicinal fields as nanocarriers for drug delivery and agents for multifunctional diagnosis,
45 for example [1,2]. Recently, a new class of carbon nanomaterials, including nanodiamonds
46 [3] and fluorescent carbon nanoparticles (CNPs) [4], have been widely investigated due to
47 their high hydrophilicity, excellent biocompatibility, good cell permeability, high
48 photostability and flexibility in surface modification as a result of the presence of different
49 functional groups (carboxyl, hydroxyl and amino groups), allowing the covalent conjugation
50 of chemotherapeutic and targeting agents [5]. Particularly, fluorescent CNPs have wide
51 applications in areas such as bioimaging, drug delivery [6–10], sensors [11–14],
52 optoelectronics [15] and photocatalysis [16]. CNPs are comparable to quantum dots (QDs)
53 and organic dyes [17]. QDs are semiconductor nanostructures with unique optical and
54 electrical properties and great flexibility in their bright and tunable photoluminescence. The
55 blinking effect is a problem with QDs that can be overcome by surface passivation or core-
56 shell formation [18]. QDs are composed of heavy metal precursors such as selenium (Se) and
57 cadmium (Cd), which are toxic at low concentrations in the human body and environment
58 [17,19]. The use of CNPs in place of QDs might overcome the above mentioned problems.
59 Notably, CNPs have attracted considerable interest, as they offer potential advantages over
60 the other carbon nanomaterials such as carbon nanotubes [20–22] and Halloysite nanotubes
61 [23,24] including their small size, simple and inexpensive synthetic routes, high aqueous
62 solubility, their fluorescence property which make them useful for cell imaging and their high
63 cargo loading.

64 In recent years, much progress has been made in terms of the synthesis, properties and
65 applications of CNPs [17,25]. The synthesis of CNPs can be classified in two groups:
66 chemical and physical methods. Chemical methods include electrochemical synthesis [26],

67 acidic oxidation [4,6,27], thermal/hydrothermal synthesis [28–31] and microwave/ultrasonic
68 synthesis [12,17,28,32]. Physical methods include arc discharge [33], laser ablation [34] and
69 plasma treatment [35]. Chemical oxidation was commonly used to prepare fluorescent CNPs,
70 which almost always originate from carbon-based nanomaterials. This method is easier,
71 avoids multi-step synthesis and introduces carboxyl and hydroxyl groups on the CNP surface,
72 making the particles negatively charged and hydrophilic. As a result, a variety of fluorescent
73 CNPs have been prepared using food waste [36], carbon nanotubes [37], candle soot [4],
74 carbohydrates (sucrose, glucose) [30,38], active carbon [32], orange juice, [polyphenol](#)
75 [39,40] and honey [41]. Although numerous synthetic approaches have been developed, those
76 that are eco-friendly and inexpensive are in demand. Furthermore, large-scale synthesis and
77 size-controlled CNPs remain unmet technological needs.

78 In the field of drug delivery, carbon nanomaterials have gained considerable attention as
79 nano-carriers due to their high surface area, enhanced cellular uptake and easy conjugation
80 with therapeutics [42–45]. CNPs are spherical and composed of an sp^2 carbon core, which
81 can be conjugated with chemotherapeutic drugs and biomolecules through covalent or
82 noncovalent interactions (π – π stacking or electrostatic interactions) and used for *in vitro* and
83 *in vivo* drug delivery applications [43,46]. However, most of the published papers to date on
84 this topic have focused on the optical properties and *in vitro* biocompatibility of CNPs [47–
85 50], and few have studied CNPs as delivery agents in depth [9,51,52]. Therefore, clinical
86 application remains a challenge.

87 In this report, we present a green source, “black tea”, as a suitable precursor for the synthesis
88 of CNPs by nitric acid (HNO_3) oxidation. This synthesis is simple and economical because of
89 the selection of an inexpensive carbon source. These CNPs are non-toxic; easily synthesized
90 in large-scale production with tunable optical properties up to red spectra, which can be
91 utilized for multiplexing applications; and can efficiently deliver doxorubicin (doxo). The

92 biodistribution, pharmacokinetics (PK) profiles and kinetics of release suggest that CNPs-
93 doxorubicin (Cdoxo) is an optimal drug delivery vector for cancer therapy.

94 **Experimental Section**

95 **Materials and Instrumentation**

96 **Reagents**

97 Commercially available Brooke Bond Taaza tea was utilized. HNO₃ (70%) and sodium
98 hydroxide (NaOH) were purchased from Sigma Aldrich (St. Louis, Missouri, US), doxo was
99 obtained from Accord Healthcare Ltd. (Durham, NC, US) and daunorubicin was purchased
100 from Teva Pharmaceutical Industries Ltd. (Petah Tikva, Israel). All reagents were used as
101 received without further purification. Minisart[®] syringe filters with a pore size of 0.2 μm
102 were from Sartorius Stedim Biotech (Concord, CA, US), and a dialysis membrane (MWCO
103 0.5-1 kDa) was purchased from Spectrum Laboratories (Rancho Dominguez, CA, US) for
104 CNP purification. LysoTracker[®] deep red probe was purchased from Life Technologies
105 (Carlsbad, CA, US). Exosomes were prepared from exosome-depleted medium conditioned
106 for 48 hours and purified with an AB cell culture-nanovesicle solution according to the
107 instructions (AB ANALITICA, Padova, Italy) [53].

108 DLD-1 and LoVo (colon) and MDA-MB-231 (breast) and HeLa (cervical) cancer cells were
109 grown as indicated by the supplier (ATCC, Manassas, VA, US). Nude and FVB mice were
110 purchased from Harlan Laboratories (Udine, Italy); the procedures were approved by the
111 Italian Ministry of Health n°788/2015-PR and performed in accordance with the institutional
112 guidelines. Data are reported as the mean and standard error.

113 **Equipment**

114 Water was obtained from a Milli-Q water purification system (18.2 Ω; EMD Millipore,
115 Billerica, MA, US). UV-Vis absorption spectra were collected using a NanoDrop 2000c
116 (Thermo Fischer Scientific, Waltham, MA, US). Fluorescence spectra were collected on an
117 Infinite M1000 PRO and cell viability analyzed using an Infinite 200 PRO (Tecan,
118 Männedorf, Switzerland). X-ray diffraction (XRD) data were collected on a Philips X'Pert

119 vertical goniometer with Bragg-Brentano geometry. Transmission electron microscopy
120 (TEM) was carried out using a Philips EM 208 microscope (Philips, Amsterdam,
121 Netherlands). Fourier transform infrared (FT-IR) spectra were obtained on a NEXUS FT-IR
122 spectrometer implementing a Nicolet Avatar diffuse reflectance accessory. X-ray
123 photoelectron spectroscopy (XPS) was performed on a PHI Quantera SXM spectrometer
124 using monochromatic Al-K α X-ray sources at 1486.6 eV and 24.8 W with a beam diameter
125 of 100.0 μ m, a 1.2 V and 20.0 μ A neutralizer, and FAT analyzer mode. Zeta potential (ζ)
126 measurements were collected on a Zetasizer ZS90 (Malvern Instruments, Malvern, UK) using
127 a 632 nm He-Ne laser as the light source. Fluorescence microscopy was carried out using a
128 Nikon microscope at 20x and 40x magnification (Nikon, Chiyoda, Tokyo, Japan). The PK
129 and biodistribution were evaluated by liquid chromatography-tandem mass spectrometry
130 (LC-MS/MS) on a 4000 QTRAP MS/MS system equipped with a Turbo ESI source (AB
131 Sciex, MA, USA). The exosome particle size was determined with an L10 NanoSight
132 instrument (Malvern Instruments Ltd, UK).

133 **Preparation of CNPs**

134 CNPs were synthesized from tea in the following steps: (1) carbonization of commercial tea
135 followed by (2) oxidation with HNO₃. The carbonized carbon was prepared by heating the
136 commercial black tea at 200 °C for approximately 3 hours, followed by evaporation of water
137 and heating again at 200 °C for approximately 5 hours. The so-formed carbonized tea powder
138 was cooled to room temperature, dried on rotary evaporator and stored in a glass bottle. Then,
139 500 mg of the carbonized carbon was dispersed in HNO₃ (0.065 mol, 5 M, 13 ml) and
140 refluxed at 80 °C for 20 hours under vigorous stirring. Then, the orange solution was cooled
141 to room temperature and centrifuged (4300g, 25 min, room temperature) to separate out any
142 unreacted carbon. The orange supernatant was collected, neutralized by 5 M NaOH and
143 filtered through a 0.2 μ m Minisart[®] syringe. To remove salts and impurities, the raw solution
144 was dialyzed against Milli-Q water using a dialysis membrane (MWCO 0.5-1 kDa) for at

145 least 2 days. Finally, the obtained golden-yellow solution was dried on a rotary evaporator
146 and used for further characterization (yield: 26%).

147 **Fluorescence imaging**

148 A droplet of an aqueous CNP dispersion (25 mg/ml) was imaged on a Nikon fluorescence
149 microscope under different filter sets (nm), Ex 350/Em 460 (blue), Ex 490/Em 520 (green),
150 Ex 550/Em 570 (red) and Ex 630/Em 670 (violet), at 20x magnification.

151 **CNP cellular localization**

152 The CNP cellular internalization was evaluated by plating HeLa cells at a density of 7.5×10^4
153 cells/slide. The next day, the cells were marked with 50 nM LysoTracker[®] deep red probe
154 (Thermo Fisher, MA, US) for 2 h at 37 °C. After incubation, the cells were washed twice
155 with 1X PBS and incubated for 24 h with 2 mg/ml CNPs. After incubation, the cells were
156 washed twice with 1X PBS and fixed with 4% PFA for 10 min, and the slides were mounted
157 with Alexa FluorSave solution (Thermo Fisher Scientific, Waltham MA, US). The images
158 were obtained on a Nikon fluorescence microscope at 40x magnification using Ex 630/Em
159 670 nm filters for the lysosomes and Ex 350/Em 460 nm filters for the CNPs.

160 **Imaging of CNP-loaded exosomes**

161 To load exosomes with CNPs, HeLa cells were grown until 70% confluence, treated with 2
162 mg/mL CNPs for 2 h, washed and then incubated in exosome-free medium for 24 h. The
163 medium was collected, and the exosomes were extracted using an AB cell culture-
164 nanovesicle solution. The next day, the medium was centrifuged at 103,000g and 4 °C for 80
165 min, and the pellet was resuspended in 1X PBS. The exosomes were characterized by NTA
166 analysis (nanoparticle tracking analysis, Malvern, UK). For imaging, the exosomes loaded
167 with CNPs were spotted on a slide and analyzed with a Nikon fluorescence microscope at
168 40x magnification under different filter sets (nm): Ex 350/Em 460 (blue), Ex 490/Em 520
169 (green), Ex 550/Em 570 (red) and Ex 630/Em 670 (violet).

170 **Doxo loading efficiency and release**

171 CNPs (0.5 mg/ml) were incubated with doxo (0.25 mg/mL) in 1X PBS for 2 h at room
172 temperature. The unbound doxo was eliminated by centrifugation at 13000g for 10 min and
173 washed twice with 1X PBS. The drug loading capacity for doxo was calculated as follows:
174 (weight of loaded doxo)/(weight of CNPs). The weight of free doxo was measured on a UV-
175 Vis spectrophotometer from the absorbance at 450 nm based on a doxo standard curve, and
176 the weight of CNPs was measured from the absorbance at 289 nm based on a CNP standard
177 curve. The release of doxo and Cdoxo (50 µg/500 µL) was evaluated using a dialysis
178 membrane (15,000 MWCO) dipped into 1 L of 1X PBS at pH 7.4 or pH 5.5.

179

180 **Toxicity, cytotoxicity and apoptosis tests**

181 The toxicity of the CNPs was tested in Hela, MDA-MB-231, LoVo and DLD-1 cancer cell
182 lines. The cytotoxicity of the free doxo, CNPs and Cdoxo was tested in MDA-MB-231, LoVo
183 and DLD-1 cancer cell lines. Toxicity and cytotoxicity were evaluated by the CellTiter-Glo[®]
184 luminescence assay (Promega, Madison, Wisconsin, US) using an Infinite 200 PRO
185 instrument (Tecan, Switzerland). Cells were seeded in 96-well plates (Falcon BD, San Jose,
186 CA, US) at a density of 10³ cells/well and incubated for 24 h to allow for cell attachment.
187 The cells were incubated with doxo, CNPs, and Cdoxo at the same drug concentrations for 96
188 h. The experiments were performed in triplicate. Apoptosis was evaluated after 24 hours by
189 fluorescence-activated cell sorting (FACS; BD Biosciences, San Jose, CA, US) utilizing the
190 PE Annexin V Apoptosis Detection Kit I (BD Biosciences, San Jose, CA, US).

191 ***In vivo* CNP toxicity and efficacy**

192 This experiment was carried out using 8 weeks old female nude mice, which were
193 administered by i.v. (intravenous) injection of 4 concentrations of CNPs diluted in PBS 1X

194 (5, 10, 20 and 40 mg/kg). The body weights of the mice were monitored for more than 45
195 days.

196 To evaluate the anti-tumour efficacy of Cdoxo compared to doxo, 3×10^6 MDA-MB-231
197 cells diluted in DMEM w/o phenol red/30% matrigel HC (Corning, New York, US) were
198 inoculated in the mammary fat pad of nude mice.

199 Histopathology: The organs of the mice were collected and fixed in 10% formalin buffered
200 with PBS, embedded in paraffin, sectioned at a thickness of 3 μ m and stained with
201 hematoxylin and eosin (H&E). The tissues were analyzed with light microscopy using
202 different magnifications.

203 **PK and biodistribution**

204 The PK experiments were performed in 8 weeks old FVB mice treated with 3 mg/kg (i.v.) of
205 the drug diluted in PBS 1X, and approximately 100 μ l of blood was collected after 0.5, 1, 3,
206 6, 24, 48, 96 and 192 hours. Blood was collected from each mouse twice: from the
207 mandibular vein (live mouse) and the right ventricle of the heart (sacrificed mouse). A total
208 of 12 mice were utilized. Serum samples were stored at -80 °C. For analysis of the drug
209 tissue distribution, the mice were sacrificed at 3 and 24 hours, and their organs were washed
210 with 10 ml of cold PBS/heparin before collection. The organs were diluted in 500 μ l of 4%
211 PBS/BSA and homogenized with a Qiagen TissueRuptor for 20 sec at power 4 in ice
212 (Qiagen, Hilden, Germany).

213 The doxo concentrations in serum and tissues were measured by LC-MS/MS. The proteins
214 were precipitated with 2 volumes of cold acetonitrile containing 20 ng/ml daunorubicin as an
215 internal standard. After vortexing and spinning at 13000 rpm for 15 min at 4 °C, the cleared
216 supernatant was diluted with 2 volumes of 0.2% formic acid, and 10 μ l of the dilution were
217 injected into the LC-MS/MS system. Chromatographic separation was performed on an
218 Accucore 150-C18 column (2.6 μ m, 30x2.1 mm; Thermo Scientific, Waltham, MA USA)

219 equilibrated with 0.2% formic acid/acetonitrile (95:5) at 0.7 ml/min and maintained at 50 °C.
220 An elution gradient B from 5% to 80% acetonitrile was applied over 5 min. A 4000 QTRAP
221 MS/MS system equipped with a Turbo ESI source (AB Sciex, Framingham, MA, USA) was
222 equilibrated for 3 min in positive-ion mode. The transitions of doxo and daunorubicin were
223 monitored in multiple reaction monitoring mode at m/z 544.1→397.2 and 528.2→321.1,
224 respectively. The spray voltage was set at 5000 V, with a source temperature of 400 °C. The
225 curtain gas, nebulizer gas (gas1) and auxiliary gas (gas 2) were set at 20, 50 and 50 arbitrary
226 units, respectively. The declustering potential and collision energy voltages were set at 45 V
227 and 16 V, respectively, for both doxo and daunorubicin.

228

229 Results and Discussion

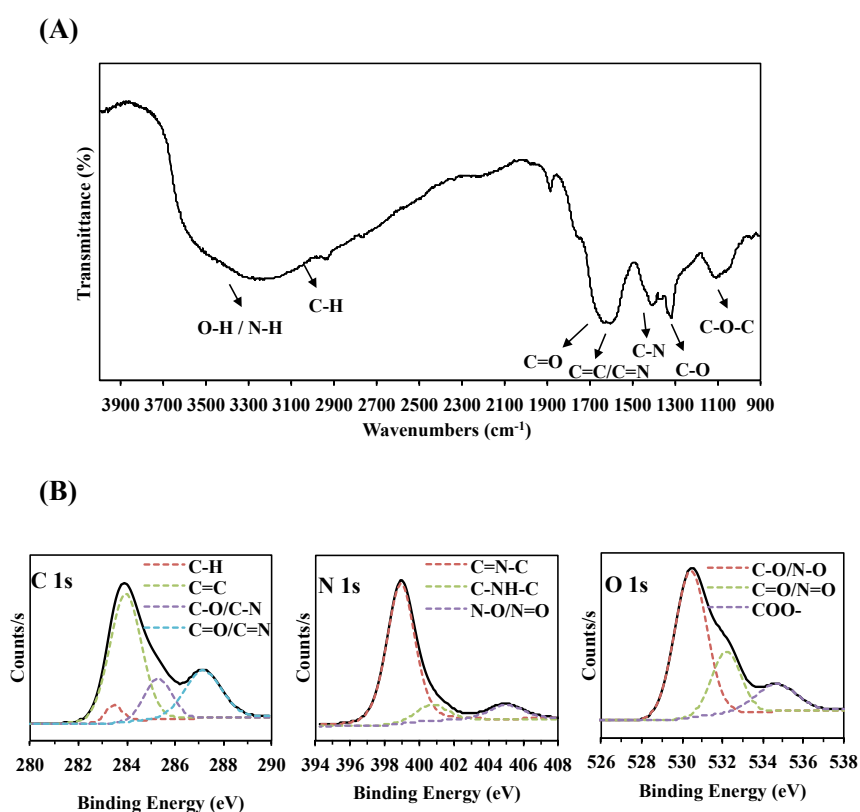
230 Characterization of CNPs prepared from black tea

231 The CNPs were prepared from tea by HNO₃ oxidation and characterized by UV-Vis
232 absorption spectroscopy, fluorescence spectroscopy, powder XRD, FT-IR spectroscopy and
233 TEM. The zeta potential of the CNPs was also measured at -16.6 mV, indicating a negative
234 charge on the CNP surface due to the presence of carboxylic groups.

235 Figure S1 shows the UV-Vis absorption and fluorescence spectra of CNPs excited at 360 nm.
236 The UV-Vis absorption spectrum contained two distinct peaks: one at 300 nm that could be
237 assigned to the n- π^* transition of the C=O groups on the surface of the CNPs and one at 242
238 nm that could be assigned to π - π^* transitions of the polycyclic aromatic systems (C=C)
239 contained in the polyphenols of the tea [54]. The CNP solution produced a maximum
240 emission peak centered at 470 nm when excited at 360 nm (Figure S1A). To investigate the
241 optical properties of the CNPs, emission spectra were recorded at various excitation
242 wavelengths from 300 to 570 nm; the emission peaks were red-shifted from 390 to 570 nm
243 while the intensities decreased (Figure S1B, S1C). These optical properties mainly result
244 from the different sizes and different distributions of emissive sites, which is generally a
245 characteristic of fluorescent carbon nanomaterials [34]. The fluorescence properties of CNPs
246 are always dependent on the size and the presence of organic functional groups in the carbon
247 source [5].

248 We applied XRD and FT-IR analyses to identify the functional groups and the phase of the
249 CNPs. The powder XRD spectrum (Figure S2) contained a broader peak at $2\theta = 24.8^\circ$,
250 revealing an amorphous carbon phase in the CNPs. The FT-IR spectrum (Figure 1A)
251 indicated that the CNPs have many oxygen- and nitrogen-containing functional groups on
252 their surface. The broad peak centered at 3294 cm⁻¹ revealed O-H/N-H bonding, and the
253 absorptions at 2937 and 2866 cm⁻¹ could be attributed to C-H stretching vibrations.

254 Moreover, the absorption peaks at 1652 and 1752 cm^{-1} are indicative of C=O bonds. The
 255 absorptions at 1110 and 1195 cm^{-1} could be attributed to C-O-C bonds, and the absorptions at
 256 1318 and 1337 cm^{-1} confirm the presence of C-O bonds. Furthermore, the absorption peaks at
 257 1594 cm^{-1} could be attributed to the C=N and C=C groups of aromatic hydrocarbons,
 258 indicating the presence of sp^2 hybridization, whereas the absorption peaks at 1406 and 1431
 259 cm^{-1} could be related to C-N bonds. These data suggest that the CNPs were functionalized
 260 with hydroxyl, alkyl, carbonyl, carboxylic, and amine groups derived from the organic
 261 molecules in the black tea and the use of HNO_3 .



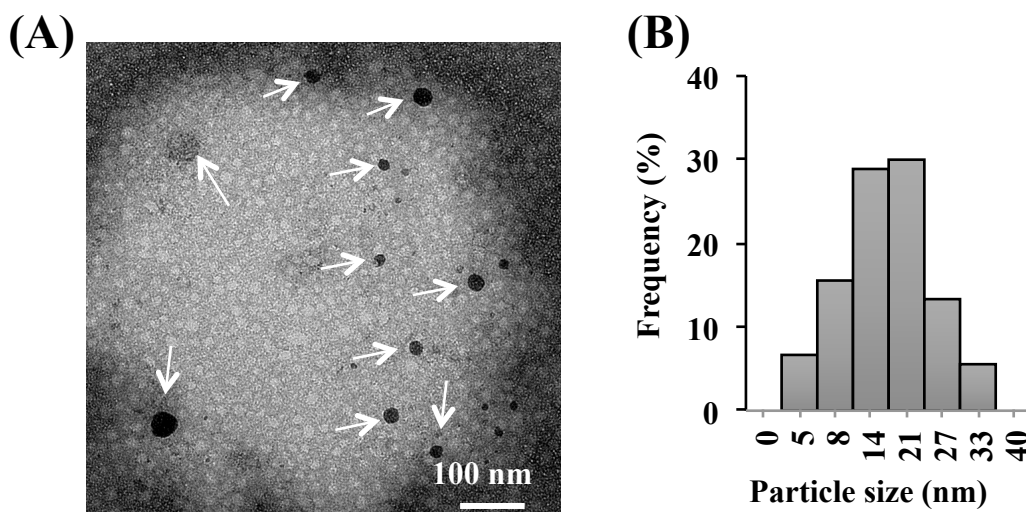
262

263 **Figure 1.** (A) FT-IR spectrum of CNPs; (B) C1s, N1s, and O1s XPS spectra.

264 XPS analysis was used to confirm the functional groups on the CNP surface. From the XPS
 265 spectrum (Figure 1B), C, N and O were detected from the peaks at 285 eV (C1s), 400.2 eV
 266 (N1s), and 532 eV (O1s), respectively, with 62.56% carbon, 31.43% oxygen, and 6.01%
 267 nitrogen. The C1s peaks at 283.5, 284, 285.3, and 287.2 eV could be assigned to carbon in
 268 the form of C-H, sp^2 (C=C), C-O/C-N and C=O/C=N, respectively [55–57]. The N1s peaks

269 consisted of three Gaussian peaks centered at 399, 408.8 and 405 eV, corresponding to C=N-
270 C, C-NH-C, and oxidized N-species such as N-O/N=O, respectively [56,57]. The O1s peaks
271 could be deconvoluted into three Gaussian peaks centered at 530.4, 532.2 and 534.7 eV,
272 corresponding to C-O/N-O, C=O/N=O, and COO⁻, respectively [57]. The surface components
273 of the CNPs are in agreement with the FTIR results. It is well known that HNO₃ oxidation
274 produces hydroxyl and carboxylic groups on CNP surfaces, which makes the particles water
275 soluble and negatively charged. In addition, this oxidation can also induce nitration [58]. Our
276 experimental data suggest that refluxing the carbonized carbon derived from tea with HNO₃
277 induces partial oxidation of the carbons; introduces functional groups, such as OH, COOH,
278 and NO₂; and causes nitrogen doping into the CNPs. The introduction of functional groups
279 imparts water solubility and a surface charge to the CNPs. This oxidation step could also be
280 considered a chemical route to incorporating nitrogen into the CNPs, as observed from the
281 chemical composition analysis.

282 The morphology and size of the CNPs were investigated by TEM. As shown in Figure 2, the
283 CNPs had a narrow size distribution and were spherical with an average diameter of 17 nm.

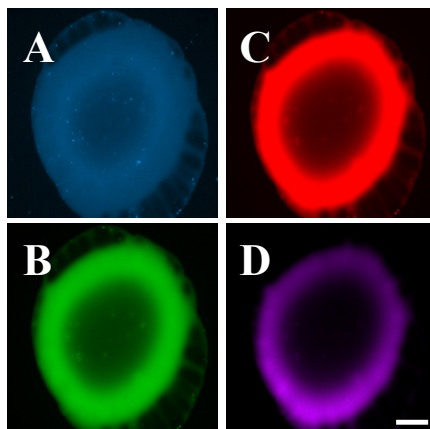


284
285 **Figure 2.** (A) TEM image and (B) particle size distribution histogram of CNPs (17.3 ± 7.6
286 nm). Arrows indicate CNPs.

287 **CNPs were biocompatible and suitable for bioimaging of cellular and subcellular**
288 **(exosomes) compartments**

289 The CNPs were reported to be not toxic in different experimental set-ups [26,59]. *In vitro*
290 experiments showed that CNPs do not alter cell viability at concentrations up to 200 µg/ml
291 [60]. A toxicity test was performed with HeLa, MDA-MB-231, LoVo and DLD-1 cells. Our
292 CNPs were not toxic at up to 1 mg/ml, illustrating very high biocompatibility (Figure S3),
293 and sustained further testing in *in vivo* experiments. To strengthen these results, an apoptosis
294 test was performed, the results of which are presented in Figure S4. Cells were treated with 1
295 mg/ml CNPs, and the expression of Annexin V on the surface of the cells was measured by
296 FACS after 24 hours. No change in the percentage of apoptotic cells was observed in the
297 CNP-treated cells over the control.

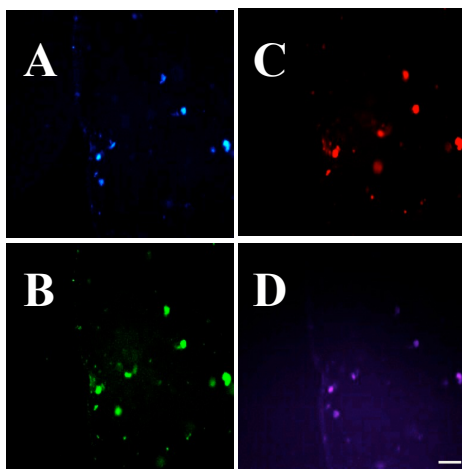
298 Although the CNPs were designed and synthesized for drug delivery applications. A droplet
299 of CNPs (25 mg/ml) was deposited on a cover slip under a fluorescent microscope and
300 imaged under different excitation wavelengths commonly utilized for biological experiments.
301 Fluorescence of the CNPs was detected in all the ranges utilized (Figure 3). For biological
302 applications, a wavelength range over 600 nm is more suitable (Figure 3D) and does not
303 overlap with the fluorescence of doxo, which has a maximal excitation/emission of
304 approximately 490/590 nm.



305

306 **Figure 3. (A-D)** Fluorescence microscopy photographs of an aqueous solution of CNPs
307 under different excitation filter sets: **(A)** 350 nm, **(B)** 490 nm, **(C)** 550 nm and **(D)** 630 nm.
308 Scale bar: 200 μm

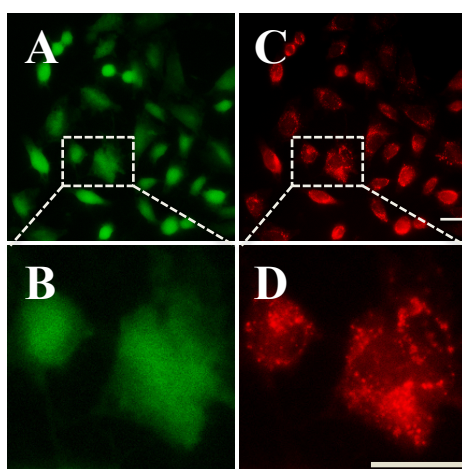
309 Due to the increasing number of papers focused on exosome biology and the possibility of
310 utilizing exosomes in liquid biopsies, the CNPs were tested for use as potential fluorescent
311 probes. Exosomes are extracellular vesicles with nanometric dimensions (30-200 nm) and
312 diagnostic [61] and therapeutic potential [62]. Exosomes incubated with CNPs were collected
313 after 24 hours and verified by NTA analysis (Figure S5). Equal quantities of exosomes were
314 evaluated under fluorescence microscopy from CNP-treated and untreated cells. A clearly
315 noticeable dotted appearance of CNP-loaded exosomes can be observed in Figure 4 and data
316 that is not shown here, suggesting that these CNPs can be utilized to probe exosomes for
317 biological applications.



318
319 **Figure 4.** Exosomes isolated from the cell culture medium of MDA-MB-231 cells treated
320 with CNPs (2 mg/ml) for 2 h and collected after 48 h. Images were acquired with different
321 excitation filter sets, as in Figure 3. Scale bar: 20 μm .

322 **CNPs avoided lysosomal entrapment and delivered doxo efficiently in *in vitro***
323 **experiments**

324 Lysosomal degradation is a natural process by which cells eliminate unnecessary endogenous
325 and exogenous materials [63]. The failure of many nanomaterials is due to their accumulation
326 inside lysosomes [64]. Escaping lysosomal degradation is a desirable functional property for
327 drug delivery applications. Under this scope, HeLa cells were probed with LysoTracker for 2
328 hours and incubated with 2 mg/ml CNPs for 24 hours. Under fluorescence microscopy, the
329 CNPs (green) had a clearly uniform distribution in the cytoplasm and nucleus, and the
330 typically punctuated appearance of lysosomal accumulation (red) was not apparently
331 observed (Figure 5).



332
333 **Figure 5.** HeLa cells (A) treated with 2 mg/ml CNPs after 24 h and marked with (C)
334 LysoTracker. (B) and (D) Zoom-in of (A) and (C). Scale bar: 20 μ m.

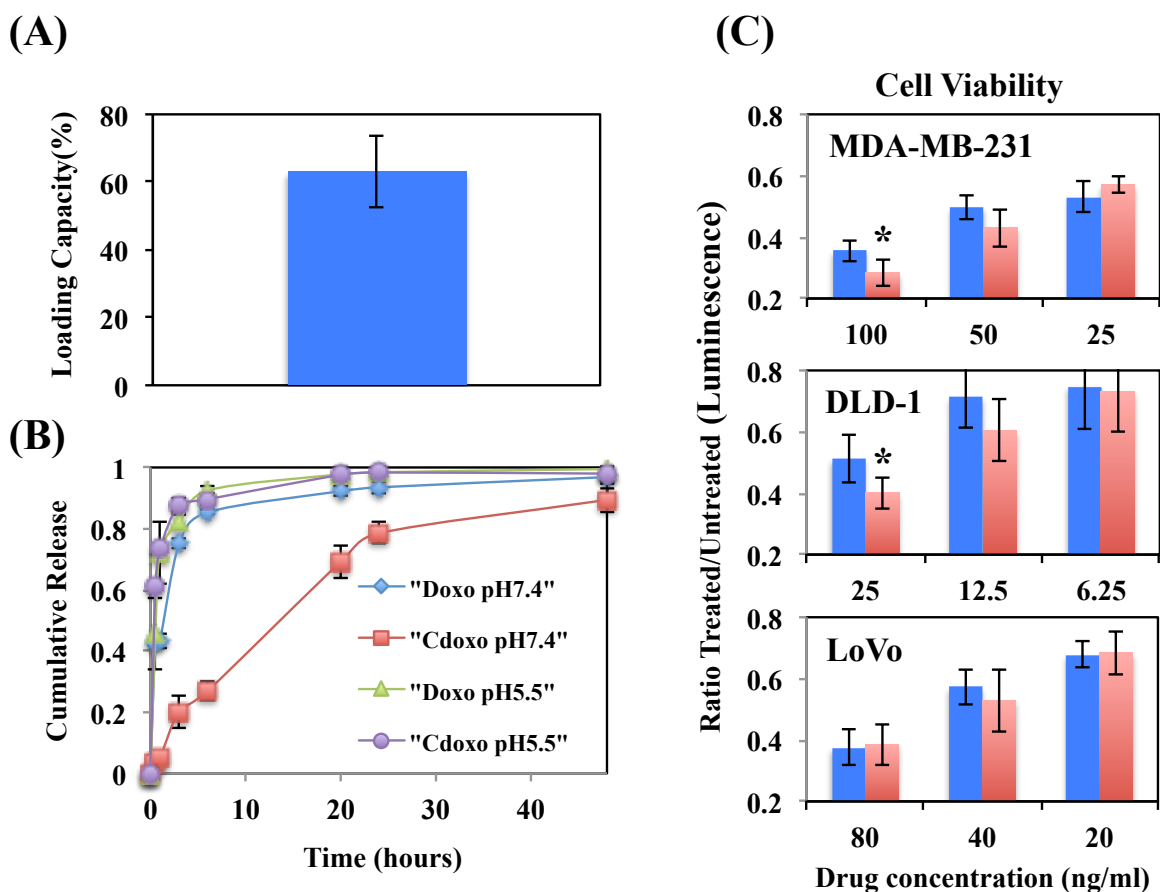
335 A desirable property of nanomaterials is an intrinsic ability for loading therapeutic drugs and
336 a controlled release over time under physiological conditions [65,66]. To demonstrate this
337 concept, the CNPs were loaded with doxo, and the kinetics of drug release was calculated
338 from a dialysis experiment in PBS at 37 °C at different pH values. For drug loading, the
339 CNPs were mixed with doxo at room temperature, and the drug loading was calculated to be
340 approximately 60% (Figure 6A). Doxo is a weak amphipathic base with $pK_a = 8.3$. At
341 physiological pH (7.4), the protonated fraction of doxo is still 10-fold that of the free base,
342 while the carboxylic acid moieties on the CNP surface are nearly completely dissociated to
343 their negative carboxylate form (pK_a range: 3-5) [67,68]. Thus, the doxo molecules retain

344 their electrostatic interactions with the CNPs at physiological pH. At pH 4, the carboxylic
345 acid groups on the CNPs are partially dissociated, decreasing the negative charge on the
346 CNPs and reducing the electrostatic interactions of the drug carrier with protonated doxo. To
347 support our conclusion, CNPs were loaded with doxo at different pH levels: 4, 5.5 and 7.4
348 (Figure S6). The percentage of loading positively correlated with the pH.

349 The extracellular pH (pHe) of tumour tissues is acidified by the metabolism of tumour cells
350 [69]. Cell survival is conditioned by maintenance of a favourable acid-base balance (pH).
351 Because of cellular metabolism, which produces CO₂ and lactic acid, cancer cells are
352 continuously exposed to large acid-base fluxes, which would disturb the pH. In contrast to
353 normal cells, most tumour cells preferentially convert glucose and other substrates to lactic
354 acid, even under aerobic conditions. This phenomenon, termed “the Warburg effect”, was
355 reported by Warburg and co-workers in the 1920s [70–72]. Due to increased glucose
356 metabolism, tumours possess a greater capacity to pump lactic acid and protons out to the
357 extracellular spaces to maintain an appropriate neutral-alkaline intracellular pH (pHi), which
358 is essential for cell vitality. The inefficient removal of protons and lactic acid from
359 extracellular spaces creates a reversed gradient characterized by an acidic pHe and alkaline
360 pHi [73–75]. *In vitro* and *in vivo* studies revealed that tumour cells have a pHi ranging from
361 7.1 to 7.6 (pHi of normal cells: 7.0 to 7.2) and a pHe of 6.2-6.9 (pHe of normal extracellular
362 space: 7.3-7.4) [76]. The intravesicular pH along the endocytic pathway ranges from pH 6.0–
363 6.5 in early endosomes to pH 4.5–5.5 in late endosomes and lysosomes [77].

364 A drug delivery system that is able to release its cargo more efficiently around the tumour
365 site at low pH (approximately pH 6) represents an intelligent system to specifically target
366 tumour cells [78]. To study the capacity and release of Cdoxo over different pH gradients, we
367 carried out a release experiment at pH 5.5 and 7.4 to mimic the bloodstream, tumour
368 microenvironments and intracellular endosome/lysosome pathway (Figure 6B) [79,80]. The
369 release of doxo was derived from a log-log plot of the cumulative release versus time.

370 Noticeably, the CNPs maintained a stable interaction with doxo at alkaline pH (pH of the
 371 bloodstream) with a slow release profile (approximately 15 hours), compared to a fast release
 372 profile (approximately 1 hour) when the medium was acidified to levels of the extracellular
 373 space of the tumour and in subcellular compartments. This pH gradient increases the ratio of
 374 the tumoral/non-tumoral drug concentration, thereby elevating the therapeutic index of doxo.
 375



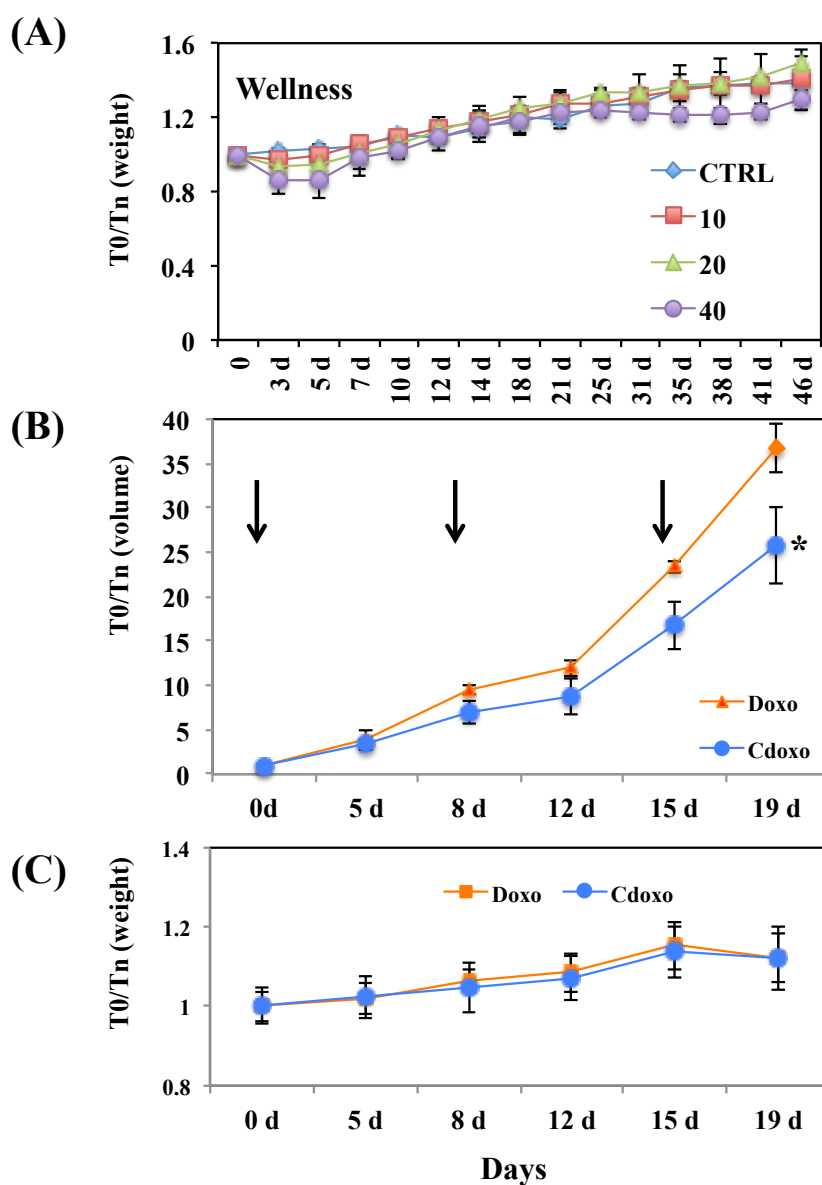
376
 377 **Figure 6.** (A) Loading capacity of Cdoxo. The graph displays the percentage of doxo loading
 378 (y-axis) (B) Release of doxo from CNPs. The cumulative release of doxo was evaluated by
 379 measuring the fluorescence of doxo, which resides inside the dialysis membrane at each time
 380 point at pH 5.5 and 7.4. (C) Cytotoxic effects of Cdoxo on MDA-MB-231, DLD-1 and LoVo
 381 cell lines treated with increasing concentrations of doxo (blue) or Cdoxo (red), as indicated
 382 on the x-axis (ng/ml). **p* value <0.05 (y-axis). The quantity of utilized doxo was based on
 383 previously calculated IC50 (middle value).

384 Subsequently, the cell viability of MDA-MB-231, LoVo and DLD-1 cells treated with Cdoxo
385 was tested. Cells were treated with 3 different concentrations of free doxo or Cdoxo, and the
386 cell viability was assessed after 96 hours (Figure 6C). Cdoxo exhibited better cytotoxicity
387 than free doxo in MDA-MB-231 and DLD-1 cells (p value < 0.05). Based on these results,
388 we further evaluated the CNPs as a drug delivery system in a mouse model of breast cancer.

389 **CNPs were not toxic in mice and increased the efficacy of doxo**

390 *In vitro* experiments demonstrated that our CNPs were not toxic at concentrations above the
391 necessary dosage for drug delivery applications. To better predict toxicity in humans, nude
392 mice were treated with a single i.v. injection of 5, 10, 20 and 40 mg/kg CNPs. Their body
393 weight was monitored as an objective parameter of mice wellness. The mice were followed
394 over a period of approximately 2 months. We did not observe any symptoms of stress or
395 clinical illness. The body weight of the mice increased during the observational period
396 (Figure 7A). After more than 6 months, the mice were sacrificed, and their tissues were
397 histopathologically analyzed. No obvious signs of toxicity were observed (Figure S7).

398 Supported by this encouraging data, MDA-MB-231 cells were orthotopically inoculated in
399 the mammary fat pad of nude mice. After the tumours had reached an average volume of 57
400 ± 8 mm³, the mice were treated 3 times on a weekly base with 3 mg/kg Cdoxo or free doxo.
401 Figure 7B demonstrates that the tumour volume of the Cdoxo-treated mice was reduced
402 compared to the tumours of mice treated with free doxo (p value < 0.05). The body weight of
403 the mice was similar among the groups of mice tested during the experiment (Figure 7C).



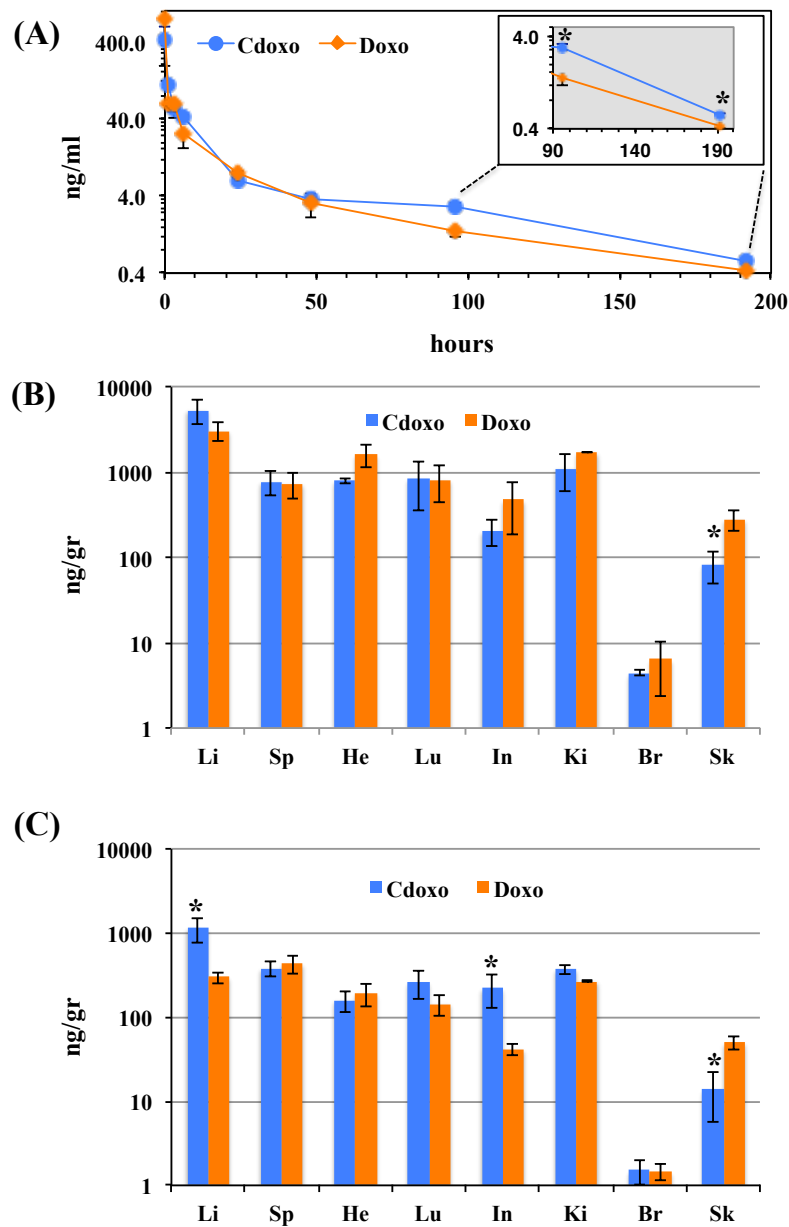
404

405 **Figure 7.** (A) Weight of mice treated with different concentrations (mg/kg) of CNPs as
 406 indicated. (B) Mice were treated 3 times (arrows) at 3 mg/kg Cdoxo or free doxo, and the
 407 tumour volume was measured (y-axis). **p* value <0.05 (C) Weight of mice treated as in (B).
 408 T_0 : time at the beginning of the experiment; T_n : time on day *n* as indicated. Eight tumours
 409 were analyzed per data point.

410 **CNPs altered the biodistribution and prolonged the circulation time of doxo**

411 Data obtained from well-known and successful liposomal formulations revealed that drug
 412 efficacy can be increased by a longer circulation time, avoiding rapid clearance [81]. To
 413 investigate the potential changes in the PK profile, we administered 3 mg/kg doxo (i.v.) and

414 Cdoxo to FVB/N mice. The PK profile of doxo in blood and tissues was qualitatively similar
 415 when administered as the free drug or Cdoxo. Both PK profiles were characterized by fast
 416 first-phase elimination. However, in the late phase of elimination, up to 4 days, the
 417 concentration of doxo in blood remained higher when administered as Cdoxo (Figure 8A)
 418 compared to free doxo. This result is consistent with the increase in the mean residence time
 419 from 14.1 ± 2 to 20.1 ± 0.5 hours (p value < 0.01) and the apparent constant elimination from
 420 0.07 ± 0.01 hour⁻¹ to 0.050 ± 0.01 hour⁻¹ (p value < 0.05) for free doxo and Cdoxo,
 421 respectively.



422

423 **Figure 8. (A)** PK profile of free doxo and Cdoxo at 0.5, 1, 3, 6, 24, 48, 96 and 192 hours. In
424 the insert, the time points 96 and 192 hours were zoomed in. **p* value <0.05. **(B) and (C)**
425 Biodistribution of free doxo and Cdoxo at 3 (B) and 24 (C) hours. At 3 hours, less Cdoxo was
426 present in the skin. At 24 hours, increased accumulation of Cdoxo in the liver and intestine
427 was observed. The y-axis is in logarithmic scale (ng/gr of drug/tissue). Li: liver, Sp: spleen,
428 He: heart, Lu: lung, In: intestine, Ki: kidney, Br: brain, Sk: skin. Three mice were utilized for
429 each data point.

430 The tissue distribution of the drug 3 hours post-injection demonstrated a similar profile
431 between Cdoxo and free doxo, except in the skin (Figure 8B). After 24 hours, the distribution
432 of Cdoxo changed, with an accumulation in the liver and intestine and a reduction in the skin
433 (*p* value < 0.05; Figure 8C). These data suggest that Cdoxo could reduce the skin toxicity
434 associated with liposomal formulations of doxo and be utilized to treat gastro-intestinal
435 cancers.

436 **Conclusions**

437 In this study, we prepared a new nanovector that can be used to image subcellular
438 compartments such as exosomes with excellent properties for drug delivery [82]. These CNPs
439 can be efficiently loaded with doxo, a widely used chemotherapeutic drug, and exhibit
440 controlled release under acidic conditions, as in the tumour microenvironment. Cdoxo was
441 more effective *in vivo* than free doxo due to a different PK profile. Hence, a simple and green
442 synthesis starting from tea could produce a tunable and safe drug delivery nanocarrier with
443 excellent biocompatible properties.

444 **References**

- 445 [1] T. Muthukumar, S. Prabhavathi, M. Chamundeeswari, T.P. Sastry, Bio-modified
446 carbon nanoparticles loaded with methotrexate possible carrier for anticancer drug
447 delivery., *Mater. Sci. Eng. C. Mater. Biol. Appl.* 36 (2014) 14–19.
448 doi:10.1016/j.msec.2013.11.046.
- 449 [2] G. Sponchia, E. Ambrosi, F. Rizzolio, M. Hadla, A. Del Tedesco, C.R. Spena, et al.,
450 Biocompatible tailored zirconia mesoporous nanoparticles with high surface area for
451 theranostic applications, *J. Mater. Chem. B.* 3 (2015) 7300–7306.
452 doi:10.1039/C5TB01424G.
- 453 [3] Y. Zhu, J. Li, W. Li, Y. Zhang, X. Yang, N. Chen, et al., The biocompatibility of
454 nanodiamonds and their application in drug delivery systems., *Theranostics.* 2 (2012)
455 302–312. doi:10.7150/thno.3627.
- 456 [4] H. Liu, T. Ye, C. Mao, Fluorescent carbon nanoparticles derived from candle soot.,
457 *Angew. Chem. Int. Ed. Engl.* 46 (2007) 6473–6475. doi:10.1002/anie.200701271.
- 458 [5] V. Kumar, G. Toffoli, F. Rizzolio, Fluorescent carbon nanoparticles in medicine for
459 cancer therapy., *ACS Med. Chem. Lett.* 4 (2013) 1012–1013. doi:10.1021/ml400394a.
- 460 [6] S.K. Bhunia, A. Saha, A.R. Maity, S.C. Ray, N.R. Jana, Carbon nanoparticle-based
461 fluorescent bioimaging probes., *Sci. Rep.* 3 (2013) 1473. doi:10.1038/srep01473.
- 462 [7] L. Cao, S.-T. Yang, X. Wang, P.G. Luo, J.-H. Liu, S. Sahu, et al., Competitive
463 performance of carbon “quantum” dots in optical bioimaging., *Theranostics.* 2 (2012)
464 295–301. doi:10.7150/thno.3912.
- 465 [8] S.E. Skrabalak, Ultrasound-assisted synthesis of carbon materials., *Phys. Chem. Chem.*
466 *Phys.* 11 (2009) 4930–4942. doi:10.1039/b823408f.
- 467 [9] H.U. Lee, S.Y. Park, E.S. Park, B. Son, S.C. Lee, J.W. Lee, et al., Photoluminescent

- 468 carbon nanotags from harmful cyanobacteria for drug delivery and imaging in cancer
469 cells., *Sci. Rep.* 4 (2014) 4665. doi:10.1038/srep04665.
- 470 [10] Q. Zeng, D. Shao, X. He, Z. Ren, W. Ji, C. Shan, et al., Carbon dots as a trackable
471 drug delivery carrier for localized cancer therapy in vivo, *J. Mater. Chem. B.* 4 (2016)
472 5119–5126. doi:10.1039/C6TB01259K.
- 473 [11] Z. Zhang, Y. Shi, Y. Pan, X. Cheng, L. Zhang, J. Chen, et al., Quinoline derivative-
474 functionalized carbon dots as a fluorescent nanosensor for sensing and intracellular
475 imaging of Zn^{2+} , *J. Mater. Chem. B.* 2 (2014) 5020. doi:10.1039/C4TB00677A.
- 476 [12] L. Zhou, Y. Lin, Z. Huang, J. Ren, X. Qu, Carbon nanodots as fluorescence probes for
477 rapid, sensitive, and label-free detection of Hg^{2+} and biothiols in complex matrices.,
478 *Chem. Commun. (Camb).* 48 (2012) 1147–1149. doi:10.1039/c2cc16791c.
- 479 [13] Q. Qu, A. Zhu, X. Shao, G. Shi, Y. Tian, Development of a carbon quantum dots-
480 based fluorescent Cu^{2+} probe suitable for living cell imaging., *Chem. Commun.*
481 (Camb). 48 (2012) 5473–5475. doi:10.1039/c2cc31000g.
- 482 [14] Y. Jiao, B. Zhu, J. Chen, X. Duan, Fluorescent sensing of fluoride in cellular system.,
483 *Theranostics.* 5 (2015) 173–187. doi:10.7150/thno.9860.
- 484 [15] L. Tang, R. Ji, X. Cao, J. Lin, H. Jiang, X. Li, et al., Deep ultraviolet
485 photoluminescence of water-soluble self-passivated graphene quantum dots., *ACS*
486 *Nano.* 6 (2012) 5102–5110. doi:10.1021/nn300760g.
- 487 [16] L. Cao, S. Sahu, P. Anilkumar, C.E. Bunker, J. Xu, K.A.S. Fernando, et al., Carbon
488 nanoparticles as visible-light photocatalysts for efficient CO_2 conversion and beyond.,
489 *J. Am. Chem. Soc.* 133 (2011) 4754–4757. doi:10.1021/ja200804h.
- 490 [17] S.N. Baker, G.A. Baker, Luminescent carbon nanodots: emergent nanolights., *Angew.*
491 *Chem. Int. Ed. Engl.* 49 (2010) 6726–6744. doi:10.1002/anie.200906623.

- 492 [18] X. Michalet, F.F. Pinaud, L.A. Bentolila, J.M. Tsay, S. Doose, J.J. Li, et al., Quantum
493 dots for live cells, in vivo imaging, and diagnostics., *Science*. 307 (2005) 538–544.
494 doi:10.1126/science.1104274.
- 495 [19] R. Hardman, A toxicologic review of quantum dots: toxicity depends on
496 physicochemical and environmental factors., *Environ. Health Perspect.* 114 (2006)
497 165–172.
- 498 [20] S. Vardharajula, S.Z. Ali, P.M. Tiwari, E. Eroğlu, K. Vig, V.A. Dennis, et al.,
499 Functionalized carbon nanotubes: biomedical applications., *Int. J. Nanomedicine*. 7
500 (2012) 5361–5374. doi:10.2147/IJN.S35832.
- 501 [21] X. Zhang, L. Meng, Q. Lu, Z. Fei, P.J. Dyson, Targeted delivery and controlled release
502 of doxorubicin to cancer cells using modified single wall carbon nanotubes.,
503 *Biomaterials*. 30 (2009) 6041–6047. doi:10.1016/j.biomaterials.2009.07.025.
- 504 [22] Z. Liu, A.C. Fan, K. Rakhra, S. Sherlock, A. Goodwin, X. Chen, et al., Supramolecular
505 Stacking of Doxorubicin on Carbon Nanotubes for In Vivo Cancer Therapy, *Angew.*
506 *Chemie Int. Ed.* 48 (2009) 7668–7672. doi:10.1002/anie.200902612.
- 507 [23] M.J. Mitchell, C.A. Castellanos, M.R. King, M.J. Mitchell, C.A. Castellanos, M.R.
508 King, Nanostructured Surfaces to Target and Kill Circulating Tumor Cells While
509 Repelling Leukocytes., *J. Nanomater.* 2012 (2012). doi:10.1155/2012/831263.
- 510 [24] M.J. Mitchell, C.S. Chen, V. Ponmudi, A.D. Hughes, M.R. King, E-selectin liposomal
511 and nanotube-targeted delivery of doxorubicin to circulating tumor cells., *J. Control.*
512 *Release*. 160 (2012) 609–617. doi:10.1016/j.jconrel.2012.02.018.
- 513 [25] J. Shen, Y. Zhu, X. Yang, C. Li, Graphene quantum dots: emergent nanolights for
514 bioimaging, sensors, catalysis and photovoltaic devices., *Chem. Commun. (Camb)*. 48
515 (2012) 3686–3699. doi:10.1039/c2cc00110a.

- 516 [26] Q.-L. Zhao, Z.-L. Zhang, B.-H. Huang, J. Peng, M. Zhang, D.-W. Pang, Facile
517 preparation of low cytotoxicity fluorescent carbon nanocrystals by electrooxidation of
518 graphite., *Chem. Commun. (Camb)*. (2008) 5116–5118. doi:10.1039/b812420e.
- 519 [27] X. Tu, Y. Ma, Y. Cao, J. Huang, M. Zhang, Z. Zhang, PEGylated carbon nanoparticles
520 for efficient in vitro photothermal cancer therapy, *J. Mater. Chem. B*. 2 (2014) 2184.
521 doi:10.1039/c3tb21750g.
- 522 [28] R. Liu, H. Li, W. Kong, J. Liu, Y. Liu, C. Tong, et al., Ultra-sensitive and selective
523 Hg²⁺ detection based on fluorescent carbon dots, *Mater. Res. Bull.* 48 (2013) 2529–
524 2534. doi:10.1016/j.materresbull.2013.03.015.
- 525 [29] Y. Guo, L. Zhang, S. Zhang, Y. Yang, X. Chen, M. Zhang, Fluorescent carbon
526 nanoparticles for the fluorescent detection of metal ions., *Biosens. Bioelectron.* 63
527 (2015) 61–71. doi:10.1016/j.bios.2014.07.018.
- 528 [30] H.K. Sadhanala, J. Khatei, K.K. Nanda, Facile hydrothermal synthesis of carbon
529 nanoparticles and possible application as white light phosphors and catalysts for the
530 reduction of nitrophenol, *RSC Adv.* 4 (2014) 11481. doi:10.1039/c3ra47527a.
- 531 [31] X. He, H. Li, Y. Liu, H. Huang, Z. Kang, S.-T. Lee, Water soluble carbon
532 nanoparticles: hydrothermal synthesis and excellent photoluminescence properties.,
533 *Colloids Surf. B. Biointerfaces.* 87 (2011) 326–332.
534 doi:10.1016/j.colsurfb.2011.05.036.
- 535 [32] H. Li, X. He, Y. Liu, H. Yu, Z. Kang, S.-T. Lee, Synthesis of fluorescent carbon
536 nanoparticles directly from active carbon via a one-step ultrasonic treatment, *Mater.*
537 *Res. Bull.* 46 (2011) 147–151. doi:10.1016/j.materresbull.2010.10.013.
- 538 [33] X. Xu, R. Ray, Y. Gu, H.J. Ploehn, L. Gearheart, K. Raker, et al., Electrophoretic
539 analysis and purification of fluorescent single-walled carbon nanotube fragments., *J.*

- 540 Am. Chem. Soc. 126 (2004) 12736–12737. doi:10.1021/ja040082h.
- 541 [34] Y.-P. Sun, B. Zhou, Y. Lin, W. Wang, K.A.S. Fernando, P. Pathak, et al., Quantum-
542 sized carbon dots for bright and colorful photoluminescence., J. Am. Chem. Soc. 128
543 (2006) 7756–7757. doi:10.1021/ja062677d.
- 544 [35] H. Jiang, F. Chen, M.G. Lagally, F.S. Denes, New strategy for synthesis and
545 functionalization of carbon nanoparticles., Langmuir. 26 (2010) 1991–1995.
546 doi:10.1021/la9022163.
- 547 [36] S.Y. Park, H.U. Lee, E.S. Park, S.C. Lee, J.-W. Lee, S.W. Jeong, et al.,
548 Photoluminescent green carbon nanodots from food-waste-derived sources: large-scale
549 synthesis, properties, and biomedical applications., ACS Appl. Mater. Interfaces. 6
550 (2014) 3365–3370. doi:10.1021/am500159p.
- 551 [37] M.H. Rummeli, A. Bachmatiuk, F. Börrnert, F. Schäffel, I. Ibrahim, K. Cendrowski, et
552 al., Synthesis of carbon nanotubes with and without catalyst particles., Nanoscale Res.
553 Lett. 6 (2011) 303. doi:10.1186/1556-276X-6-303.
- 554 [38] H. Li, X. He, Y. Liu, H. Huang, S. Lian, S.-T. Lee, et al., One-step ultrasonic synthesis
555 of water-soluble carbon nanoparticles with excellent photoluminescent properties,
556 Carbon 49 (2011) 605-609. doi:10.1016/j.carbon.2010.10.004 .
- 557 [39] S. Sahu, B. Behera, T.K. Maiti, S. Mohapatra, Simple one-step synthesis of highly
558 luminescent carbon dots from orange juice: application as excellent bio-imaging
559 agents., Chem. Commun. (Camb). 48 (2012) 8835–8837. doi:10.1039/c2cc33796g.
- 560 [40] A. Konwar, N. Gogoi, G. Majumdar, D. Chowdhury, Green chitosan-carbon dots
561 nanocomposite hydrogel film with superior properties., Carbohydr. Polym. 115 (2015)
562 238–245. doi:10.1016/j.carbpol.2014.08.021.
- 563 [41] L. Wu, M. Luderer, X. Yang, C. Swain, H. Zhang, K. Nelson, et al., Surface

- 564 passivation of carbon nanoparticles with branched macromolecules influences near
565 infrared bioimaging., *Theranostics*. 3 (2013) 677–686. doi:10.7150/thno.6535.
- 566 [42] J. Shi, H. Zhang, L. Wang, L. Li, H. Wang, Z. Wang, et al., PEI-derivatized fullerene
567 drug delivery using folate as a homing device targeting to tumor., *Biomaterials*. 34
568 (2013) 251–261. doi:10.1016/j.biomaterials.2012.09.039.
- 569 [43] F. Karchemski, D. Zucker, Y. Barenholz, O. Regev, Carbon nanotubes-liposomes
570 conjugate as a platform for drug delivery into cells., *J. Control. Release*. 160 (2012)
571 339–345. doi:10.1016/j.jconrel.2011.12.037.
- 572 [44] B.S. Wong, S.L. Yoong, A. Jagusiak, T. Panczyk, H.K. Ho, W.H. Ang, et al., Carbon
573 nanotubes for delivery of small molecule drugs., *Adv. Drug Deliv. Rev.* 65 (2013)
574 1964–2015. doi:10.1016/j.addr.2013.08.005.
- 575 [45] J. Shi, L. Wang, J. Gao, Y. Liu, J. Zhang, R. Ma, et al., A fullerene-based multi-
576 functional nanoplatform for cancer theranostic applications, *Biomaterials*. 35 (2014)
577 5771–5784. doi:10.1016/j.biomaterials.2014.03.071.
- 578 [46] M. Ajmal, U. Yunus, A. Matin, N.U. Haq, Synthesis, characterization and in vitro
579 evaluation of methotrexate conjugated fluorescent carbon nanoparticles as drug
580 delivery system for human lung cancer targeting., *J. Photochem. Photobiol. B*. 153
581 (2015) 111–120. doi:10.1016/j.jphotobiol.2015.09.006.
- 582 [47] S.-T. Yang, L. Cao, P.G. Luo, F. Lu, X. Wang, H. Wang, et al., Carbon dots for optical
583 imaging in vivo., *J. Am. Chem. Soc.* 131 (2009) 11308–9. doi:10.1021/ja904843x.
- 584 [48] S. Zhu, Q. Meng, L. Wang, J. Zhang, Y. Song, H. Jin, et al., Highly photoluminescent
585 carbon dots for multicolor patterning, sensors, and bioimaging., *Angew. Chem. Int.*
586 *Ed. Engl.* 52 (2013) 3953–3957. doi:10.1002/anie.201300519.
- 587 [49] J. Wang, P. Zhang, C. Huang, G. Liu, K.C.-F. Leung, Y.X.J. Wang, High Performance

588 Photoluminescent Carbon Dots for In Vitro and In Vivo Bioimaging: Effect of
589 Nitrogen Doping Ratios., *Langmuir*. 31 (2015) 8063–8073.
590 doi:10.1021/acs.langmuir.5b01875.

591 [50] X. Huang, F. Zhang, L. Zhu, K.Y. Choi, N. Guo, J. Guo, et al., Effect of injection
592 routes on the biodistribution, clearance, and tumor uptake of carbon dots., *ACS Nano*.
593 7 (2013) 5684–5693. doi:10.1021/nn401911k.

594 [51] A. Mewada, S. Pandey, M. Thakur, D. Jadhav, M. Sharon, Swarming carbon dots for
595 folic acid mediated delivery of doxorubicin and biological imaging, *J. Mater. Chem. B*.
596 2 (2014) 698–705. doi:10.1039/C3TB21436B.

597 [52] M. Zheng, S. Liu, J. Li, D. Qu, H. Zhao, X. Guan, et al., Integrating oxaliplatin with
598 highly luminescent carbon dots: an unprecedented theranostic agent for personalized
599 medicine., *Adv. Mater.* 26 (2014) 3554–3560. doi:10.1002/adma.201306192.

600 [53] M. Hadla, S. Palazzolo, G. Corona, I. Caligiuri, V. Canzonieri, G. Toffoli, et al.,
601 Exosomes increase the therapeutic index of doxorubicin in breast and ovarian cancer
602 mouse models., *Nanomedicine (Lond)*. 11 (2016) 2431–2441. doi:10.2217/nmm-2016-
603 0154.

604 [54] X. Wen, P. Yu, Y.-R. Toh, X. Hao, J. Tang, Intrinsic and Extrinsic Fluorescence in
605 Carbon Nanodots: Ultrafast Time-Resolved Fluorescence and Carrier Dynamics, *Adv.*
606 *Opt. Mater.* 1 (2013) 173–178. doi:10.1002/adom.201200046.

607 [55] S. Liu, J. Tian, L. Wang, Y. Luo, J. Zhai, X. Sun, et al., Preparation of
608 photoluminescent carbon nitride dots from CCl₄ and 1,2-ethylenediamine: a heat-
609 treatment-based strategy, *J. Mater. Chem.* 21 (2011) 11726. doi:10.1039/c1jm12149a.

610 [56] M. Tan, X. Li, H. Wu, B. Wang, J. Wu, N-doped carbon dots derived from bovine
611 serum albumin and formic acid with one- and two-photon fluorescence for live cell

- 612 nuclear imaging., *Colloids Surf. B. Biointerfaces.* 136 (2015) 141–149.
613 doi:10.1016/j.colsurfb.2015.09.008.
- 614 [57] S.C. Ray, A. Saha, N.R. Jana, R. Sarkar, Fluorescent Carbon Nanoparticles: Synthesis,
615 Characterization, and Bioimaging Application, *J. Phys. Chem. C.* 113 (2009) 18546–
616 18551. doi:10.1021/jp905912n.
- 617 [58] I.I. Salame, T.J. Bandosz, Surface Chemistry of Activated Carbons: Combining the
618 Results of Temperature-Programmed Desorption, Boehm, and Potentiometric
619 Titrations., *J. Colloid Interface Sci.* 240 (2001) 252–258. doi:10.1006/jcis.2001.7596.
- 620 [59] S.-T. Yang, X. Wang, H. Wang, F. Lu, P.G. Luo, L. Cao, et al., Carbon Dots as
621 Nontoxic and High-Performance Fluorescence Imaging Agents., *J. Phys. Chem. C.*
622 *Nanomater. Interfaces.* 113 (2009) 18110–18114. doi:10.1021/jp9085969.
- 623 [60] J. Ge, Q. Jia, W. Liu, L. Guo, Q. Liu, M. Lan, et al., Red-Emissive Carbon Dots for
624 Fluorescent, Photoacoustic, and Thermal Theranostics in Living Mice., *Adv. Mater.* 27
625 (2015) 4169–4177. doi:10.1002/adma.201500323.
- 626 [61] S.A. Melo, L.B. Luecke, C. Kahlert, A.F. Fernandez, S.T. Gammon, J. Kaye, et al.,
627 Glypican-1 identifies cancer exosomes and detects early pancreatic cancer, *Nature.*
628 523 (2015) 177–182. doi:10.1038/nature14581.
- 629 [62] G. Toffoli, M. Hadla, G. Corona, I. Caligiuri, S. Palazzolo, S. Semeraro, et al.,
630 Exosomal doxorubicin reduces the cardiac toxicity of doxorubicin., *Nanomedicine*
631 (Lond). 10 (2015) 2963-2971. doi:10.2217/nnm.15.118.
- 632 [63] E.-L. Eskelinen, P. Saftig, Autophagy: A lysosomal degradation pathway with a
633 central role in health and disease, *Biochim. Biophys. Acta - Mol. Cell Res.* 1793
634 (2009) 664–673. doi:10.1016/j.bbamcr.2008.07.014.
- 635 [64] D. Huang, H. Zhou, J. Gao, Nanoparticles modulate autophagic effect in a dispersity-

- 636 dependent manner., *Sci. Rep.* 5 (2015) 14361. doi:10.1038/srep14361.
- 637 [65] J. Wolfram, H. Shen, M. Ferrari, Multistage vector (MSV) therapeutics., *J. Control.*
638 *Release.* 219 (2015) 406–415. doi:10.1016/j.jconrel.2015.08.010.
- 639 [66] E. Blanco, H. Shen, M. Ferrari, Principles of nanoparticle design for overcoming
640 biological barriers to drug delivery, *Nat. Biotechnol.* 33 (2015) 941–951.
641 doi:10.1038/nbt.3330.
- 642 [67] B.G. Tehan, E.J. Lloyd, M.G. Wong, W.R. Pitt, J.G. Montana, D.T. Manallack, et al.,
643 Estimation of pKa Using Semiempirical Molecular Orbital Methods. Part 1:
644 Application to Phenols and Carboxylic Acids., *Quant. Struct. Relationships.* 21 (2002)
645 457–472. doi:10.1002/1521-3838(200211)21:5<457::AID-QSAR457>3.0.CO;2-5.
- 646 [68] J. Reijenga, A. van Hoof, A. van Loon, B. Teunissen, Development of Methods for the
647 Determination of pKa Values., *Anal. Chem. Insights.* 8 (2013) 53–71.
648 doi:10.4137/ACI.S12304.
- 649 [69] Y. Kato, S. Ozawa, C. Miyamoto, Y. Maehata, A. Suzuki, T. Maeda, et al., Acidic
650 extracellular microenvironment and cancer., *Cancer Cell Int.* 13 (2013) 89.
651 doi:10.1186/1475-2867-13-89.
- 652 [70] M.G. Vander Heiden, L.C. Cantley, C.B. Thompson, Understanding the Warburg
653 effect: the metabolic requirements of cell proliferation., *Science.* 324 (2009) 1029–
654 1033. doi:10.1126/science.1160809.
- 655 [71] R.A. Gatenby, R.J. Gillies, Why do cancers have high aerobic glycolysis?, *Nat. Rev.*
656 *Cancer.* 4 (2004) 891–899. doi:10.1038/nrc1478.
- 657 [72] O. Warburg, F. Wind, E. Negelein, THE METABOLISM OF TUMORS IN THE
658 BODY., *J. Gen. Physiol.* 8 (1927) 519–530.
- 659 [73] L.E. Gerweck, K. Seetharaman, Cellular pH gradient in tumor versus normal tissue:

- 660 potential exploitation for the treatment of cancer., *Cancer Res.* 56 (1996) 1194–8.
- 661 [74] A. Hulikova, A.L. Harris, R.D. Vaughan-Jones, P. Swietach, Regulation of
662 intracellular pH in cancer cell lines under normoxia and hypoxia., *J. Cell. Physiol.* 228
663 (2013) 743–752. doi:10.1002/jcp.24221.
- 664 [75] A.I. Hashim, X. Zhang, J.W. Wojtkowiak, G. V Martinez, R.J. Gillies, Imaging pH
665 and metastasis., *NMR Biomed.* 24 (2011) 582–591. doi:10.1002/nbm.1644.
- 666 [76] M. V Shirmanova, I.N. Druzhkova, M.M. Lukina, M.E. Matlashov, V. V Belousov,
667 L.B. Snopova, et al., Intracellular pH imaging in cancer cells in vitro and tumors in
668 vivo using the new genetically encoded sensor SypHer2., *Biochim. Biophys. Acta.*
669 1850 (2015) 1905–1911. doi:10.1016/j.bbagen.2015.05.001.
- 670 [77] A. Sorkin, M. Von Zastrow, Signal transduction and endocytosis: close encounters of
671 many kinds., *Nat. Rev. Mol. Cell Biol.* 3 (2002) 600–614. doi:10.1038/nrm883.
- 672 [78] Z. Wang, J. Xia, C. Zhou, B. Via, Y. Xia, F. Zhang, et al., Synthesis of strongly green-
673 photoluminescent graphene quantum dots for drug carrier., *Colloids Surf. B.*
674 *Biointerfaces.* 112 (2013) 192–196. doi:10.1016/j.colsurfb.2013.07.025.
- 675 [79] A.R. Chowdhuri, T. Singh, S.K. Ghosh, S.K. Sahu, Carbon Dots Embedded Magnetic
676 Nanoparticles @Chitosan @Metal Organic Framework as a Nanoprobe for pH
677 Sensitive Targeted Anticancer Drug Delivery., *ACS Appl. Mater. Interfaces.* 8 (2016)
678 16573–16583. doi:10.1021/acsami.6b03988.
- 679 [80] Z. Liu, X. Sun, N. Nakayama-Ratchford, H. Dai, Supramolecular chemistry on water-
680 soluble carbon nanotubes for drug loading and delivery., *ACS Nano.* 1 (2007) 50–56.
681 doi:10.1021/nn700040t.
- 682 [81] A.T. Horowitz, Y. Barenholz, A.A. Gabizon, In vitro cytotoxicity of liposome-
683 encapsulated doxorubicin: dependence on liposome composition and drug release.,

684 Biochim. Biophys. Acta. 1109 (1992) 203–209. doi:10.1016/0005-2736(92)90084-Y.
685 [82] S. Kunjachan, J. Ehling, G. Storm, F. Kiessling, T. Lammers, Noninvasive Imaging of
686 Nanomedicines and Nanotheranostics: Principles, Progress, and Prospects., Chem.
687 Rev. 115 (2015) 10907–10937. doi:10.1021/cr500314d.

688

689

690 **Funding Sources**

691 My First AIRC (No. 1569)

692 AIRC Special Program Molecular Clinical Oncology, 5x1000, (No. 12214)

693 Italian Ministry of Education MIUR (FIRB prot. RBAP11ETKA)

694

695 **Acknowledgements**

696 The authors are thankful to My First AIRC (No. 1569); AIRC Special Program Molecular

697 Clinical Oncology, 5x1000, (No. 12214); and Italian Ministry of Education MIUR (FIRB

698 prot. RBAP11ETKA) for funding.

699 **Competing Interests**

700 The authors declare no competing interests.